Published OnlineFirst December 27, 2017; DOI: 10.1158/0008-5472.CAN-17-3303

Tumor Biology and Immunology

Cancer Research

Combined Mutation of *Apc, Kras*, and *Tgfbr2* Effectively Drives Metastasis of Intestinal Cancer

Eri Sakai[1,2], Mizuho Nakayama[1,2], Hiroko Oshima[1,2], Yuta Kouyama[3], Atsushi Niida[4], Satoshi Fujii[5], Atsushi Ochiai[6], Keiichi I. Nakayama[7], Koshi Mimori[3], Yutaka Suzuki[8], Chang Pyo Hong[9], Chan-Young Ock[9,10], Seong-Jin Kim[9,10], and Masanobu Oshima[1,2,11]

Abstract

Colorectal cancer is driven by the accumulation of driver mutations, but the contributions of specific mutations to different steps in malignant progression are not fully understood. In this study, we generated mouse models harboring different combinations of key colorectal cancer driver mutations (*Apc, Kras, Tgfbr2, Trp53, Fbxw7*) in intestinal epithelial cells to comprehensively investigate their roles in the development of primary tumors and metastases. $Apc^{\Delta 716}$ mutation caused intestinal adenomas and combination with $Trp53^{R270H}$ mutation or *Tgfbr2* deletion induced submucosal invasion. The addition of $Kras^{G12D}$ mutation yielded epithelial–mesenchymal transition (EMT)-like morphology and lymph vessel intravasation of the invasive tumors. In contrast, combinations of $Apc^{\Delta 716}$ with $Kras^{G12D}$ and *Fbxw7* mutation were insufficient for submucosal invasion, but still induced EMT-like histology. Studies using tumor-derived organoids showed that $Kras^{G12D}$ was critical for liver metastasis following splenic transplantation, when this mutation was combined with either $Apc^{\Delta 716}$ plus $Trp53^{R270H}$ or *Tgfbr2* deletion, with the highest incidence of metastasis displayed by tumors with a $Apc^{\Delta 716}$ $Kras^{G12D}$ $Tgfbr2^{-/-}$ genotype. RNA sequencing analysis of tumor organoids defined distinct gene expression profiles characteristic for the respective combinations of driver mutations, with upregulated genes in $Apc^{\Delta 716}$ $Kras^{G12D}$ $Tgfbr2^{-/-}$ tumors found to be similarly upregulated in specimens of human metastatic colorectal cancer. Our results show how activation of Wnt and Kras with suppression of TGFβ signaling in intestinal epithelial cells is sufficient for colorectal cancer metastasis, with possible implications for the development of metastasis prevention strategies.

Significance: These findings illuminate how key driver mutations in colon cancer cooperate to drive the development of metastatic disease, with potential implications for the development of suitable prevention strategies. *Cancer Res; 78(5); 1334–46. ©2017 AACR.*

Introduction

Colorectal cancer is a leading cause of cancer-related death worldwide (1, 2), and the 5-year survival rate drops significantly to about 14% for patients with metastasis (3). It is therefore extremely important to clarify the biological mechanisms of malignant progression to identify novel therapeutic target pathways. The gradual accumulation of genetic alterations in driver genes is known to cause development and malignant progression of colorectal cancer and is an established concept of multistep tumorigenesis (4, 5). Recent genome-wide analyses have confirmed the presence of frequently mutated driver genes in human colorectal cancer (6, 7). Using organoid culture systems, it has been shown that the introduction of genetic alterations in driver genes, *APC, KRAS, SMAD4, TP53*, and *PIK3A*, in intestinal epithelial cells induces tumorigenesis (8–10).

These driver mutations are classified as cancer signaling pathways (11), and the possible mechanisms of each mutation in tumorigenesis have been well studied. For example, loss of *APC* results in Wnt signaling activation, leading to the acquisition of stemness (12). KRAS plays a major role in tumorigenesis through the activation of RAF–MAPK and PI3K pathways (13). In contrast, TGFβ signaling promotes differentiation of epithelial cells, thus playing a tumor suppressor role in colorectal cancer (14). Furthermore, FBXW7 is a component of the ubiquitin ligase complex that degrades proto-oncogene products, thereby functioning as a tumor suppressor (15), and the disruption of *Fbxw7* promotes intestinal tumorigenesis (16, 17). Recent results indicate that mutant p53 alters the gene expression globally by gain-of-function mechanism, which promotes tumorigenesis (18, 19).

Moreover, the effects of simultaneous mutations in combination on colorectal cancer have also been genetically studied. It has

[1]Division of Genetics, Cancer Research Institute, Kanazawa University, Kanazawa, Japan. [2]AMED-CREST, AMED, Japan Agency for Medical Research and Development, Tokyo, Japan. [3]Department of Surgery, Kyushu University Beppu Hospital, Beppu, Japan. [4]Division of Health Medical Computational Science, Health Intelligence Center, Institute of Medical Science, The University of Tokyo, Tokyo, Japan. [5]Division of Pathology, Exploratory Oncology Research and Clinical Trial Center, National Cancer Center, Kashiwa, Japan. [6]Exploratory Oncology Research and Clinical Trial Center, National Cancer Center, Kashiwa, Japan. [7]Department of Molecular and Cellular Biology, Medical Institute of Bioregulation, Kyushu University, Fukuoka, Japan. [8]Department of Computational Biology and Medical Sciences, Graduate School of Frontier Sciences, University of Tokyo, Chiba, Japan. [9]Theragen Etex Bio Institute, Suwon, Korea. [10]Precision Medicine Research Center, Advanced Institutes of Convergence Technology and Department of Transdisciplinary Studies, Graduate School of Convergence Science and Technology, Seoul National University, Suwon, Korea. [11]Nano Life Science Institute (Nano LSI), Kanazawa University, Kanazawa, Japan.

Note: Supplementary data for this article are available at Cancer Research Online (http://cancerres.aacrjournals.org/).

E. Sakai and M. Nakayama contributed equally to this article.

Corresponding Author: Masanobu Oshima, Division of Genetics, Cancer Research Institute, Kanazawa University, Kanazawa 920-1192, Japan. Phone: 81-76-264-6760; Fax: 81-76-234-4519; E-mail: oshimam@staff.kanazawa-u.ac.jp

doi: 10.1158/0008-5472.CAN-17-3303

Published OnlineFirst December 27, 2017; DOI: 10.1158/0008-5472.CAN-17-3303

been shown that the suppression of TGFβ pathway or expression of mutant p53 in $Apc^{\Delta 716}$ mice induces the submucosal invasion of intestinal tumors (20–22). Moreover, the *Kras* mutation in addition to *Apc* and *Trp53* mutation causes invasion and metastasis (23, 24). However, despite these findings from genetic studies, the big picture regarding how specific combinations of driver mutations promote each step of malignant progression in the primary tumors and metastatic foci remains unclear.

In this study, we generated mouse models carrying the $Apc^{\Delta 716}$ mutation together with conditional mutant alleles of $Kras^{G12D}$, $Trp53^{R270H}$, $Tgfbr2^{-/-}$, or $Fbxw7^{-/-}$ in various combinations and examined their intestinal tumor phenotypes. Using these mouse models and allografts of tumor-derived organoids, we found the specific combinations of the driver mutations that were responsible for submucosal invasion, epithelial–mesenchymal transition (EMT)-like morphology, intravasation, and metastasis. Particularly, the combinations including $Apc^{\Delta 716}$ $Kras^{G12D}$ $Tgfbr2^{-/-}$ mutations caused efficient liver metastasis. Moreover, RNA sequencing (RNA-Seq) analysis corroborated the distinct expression profiles for the specific mutational combinations that are associated with distinct malignant phenotypes in both mice and human. Accordingly, targeting the pathways that regulate specific progression processes will be effective for the prevention of colorectal cancer metastasis.

Materials and Methods

Mouse experiments

$Apc^{\Delta 716}$, $Fbxw7^{flox/flox}$, and *villin-CreER* mice were described previously (25–27). $Tgfbr2^{flox/flox}$, $Trp53^{LSL\text{-}R270H}$, and $Kras^{LSL\text{-}G12D}$ mice were obtained from the Mouse Repository (NCI-Frederick, Frederick, MD; refs. 28–30). Primer sequences for genotyping are previously reported except for *Trp53* forward primer, 5′-CCTGCCAGCTCCGAAAGATT-3′. The genetic background of all strains used in this study is C57BL/6. All mice were treated with tamoxifen intraperitoneally at 4 mg/mouse once a week from 8 weeks of age for 4 weeks. For the survival curve analysis, mice were observed until 270 days of age, and the mice were euthanized when they showed a moribund phenotype. The total numbers of polyps in both the small intestine and colon were scored at 13–16 weeks of age (n = 3–5 for each genotype). NOD/Shi-*scid* $Il2rg^{-/-}$ mice (NSG mice) and C57BL/6 mice were purchased (CIEA). All animal experiments were performed with the protocol approved by the Committee on Animal Experimentation of Kanazawa University.

Histology and IHC

The primary intestinal tumors and liver metastasized tumors were fixed in 4% paraformaldehyde, paraffin-embedded, and sectioned at 4-μm thickness. The sections were stained with hematoxylin and eosin (H&E) or Masson's trichrome stain. Antibodies against E-cadherin (R&D Systems), αSMA (Sigma), F4/80 (Serotec), CD3ε (Santa Cruz Biotechnology), Ki67 (Life Technology), Lyve-1 (Acris Antibodies GmbH), vWF (DakoCytomation, Denmark), Snail2 (Bioss), CD4, CD8, and CD45R (BD Pharmingen) were used as the primary antibody. Staining signals were visualized using the Vectastain Elite Kit (Vector Laboratories). For fluorescent IHC, Alexa Fluor 594- or Alexa Fluor 488–conjugated antibodies (Molecular Probes) were used as the secondary antibody. The histologic classification of the tumors was performed according to the Japanese Classification of Colorectal Carcinoma (31).

The mean Ki67-labeling indices were calculated as the number of Ki67-positive cells per total number of tumor cells by counting 5 independent microscopic fields (×200) for three independent tumors per mouse (n = 3) or 3–8 independent foci of liver metastasized tumors (NSG mice n = 3 for each, C57BL/6 mice n = 1–5).

The immunostaining-positive areas for F4/80, αSMA and CD3ε in the microscopic fields were measured using the Hybrid cell count software program of All-In-One microscope (Keyence). For the primary tumors, the ratio of the αSMA immunostaining-positive area was calculated from 3–5 polyps per mouse (n = 3). For the liver metastasized tumors, the ratios of αSMA, F4/80, and CD3ε immunostaining-positive areas were calculated from 3 to 12 foci per mouse (NSG mice n = 3, C57BL/6 mice n = 1–5).

Scoring invasion efficiency and solitary cells

The total numbers of invading polyps in submucosa and total polyps were counted on the H&E-staining sections of whole intestine and the invasion efficiency was calculated (n = 4–5). Solitary tumor cells were detected by IHC for E-cadherin, and the numbers of solitary cells were counted on the sections (n = 4–18) while the mean numbers were calculated per 1-mm^2 area using the Hybrid cell count software program (Keyence).

Organoid culture and transplantation experiments

The organoid cultures were prepared from small intestinal tumors, as described previously (22). Authentication of the organoid cells was done by genotyping for the respective combined mutations. Cryopreserved stocks were established after testing, and experiments were performed within 5–10 passages following thaw of frozen stocks. Mycoplasma testing was done by indirect immunofluorescence test and nested PCR. The cultured organoids were mechanically dissociated, and 3×10^5 organoid cells were injected with Matrigel into the spleen of NSG mice (n = 3–5) or C57BL/6 mice (n = 4–18). At four weeks after transplantation, the liver and lung were examined histologically. The multiplicity of metastatic foci in the liver was scored by the measurement of the metastasized tumor areas on H&E sections and the calculated percentages per total liver (NSG, n = 3–5; C57BL/6, n = 5–12).

Next-generation RNA sequencing

Total RNA was extracted from organoid cells using an RNeasy plus Micro kit (Qiagen). RNA-Seq Libraries were prepared using a SureSelect Strand Specific RNA Reagent Kit (Agilent Technologies) according to the manufacturer's protocol. Thirty-six bp of single-end sequencing was performed using an Illumina HiSeq3000 (Illumina). Obtained reads were aligned to UCSC mm10 using tophat2. For the expression estimation, we counted the number of reads, which uniquely mapped to the exon of RefSeq transcripts, and calculated the reads per kilo-base of exon model per million mapped reads (RPKM) as the expression value. The sequencing data were deposited in the DNA Data Bank of Japan (DDBJ, accession #DRA005647). Clean reads that average quality scores for all libraries were more than Q30 were aligned to the mouse reference (Ensembl 85) using TopHat2 (32).

Hierarchical clustering and GO term analysis

Gene expression quantification was performed using Cufflinks (33). Differential expression analysis between samples with

Published OnlineFirst December 27, 2017; DOI: 10.1158/0008-5472.CAN-17-3303

replicates was performed using Cuffdiff with the cut-off set at $P < 0.01$ and ≥ 1.5-fold change. Hierarchical clustering for selected genes were analyzed with MeV (http://mev.tm4.org) using Euclidean distance and complete linkage method. Functional annotation for module members were performed by DAVID (34), and relevant gene ontology (GO) terms were selected with a cutoff of $P < 0.01$.

Processing genomic data from The Cancer Genome Atlas project

We used publicly available, level 3 data of The Cancer Genome Atlas (TCGA) in the current study. Clinical information and mRNA expression data obtained by RNA-seq of the TCGA samples were downloaded from the USCS Cancer Browser (https://genome-cancer.ucsc.edu). The patients' clinical data and molecular subtype status of the tumors were referred from the TCGA database (6). Among colorectal cancer samples, 343 tumor samples that included RNAseq data and metastasis information (M0, $n = 285$; M1, $n = 58$) were analyzed for the current study.

The principal component analysis

The RPKM values from RNA-seq of intestinal tumor organoids were subjected to quantile normalization and 5,000 genes with the highest variances were input to principal component analysis (PCA). PCA was performed using the prcomp function implemented in the R software (https://www.r-project.org).

Statistical analysis

The data were analyzed using an unpaired t test and are presented as the means ± SD. A value of $P < 0.05$ was considered as statistically significant. The significance of the differences of RNA expressions according to same or more than two groups was calculated by the Wilcoxon rank-sum test. For RNA-seq data, statistical analyses and data presentations were performed in R language 3.1.3 (http://www.r-project.org)

Results

Generation of mouse models carrying driver mutations in combination

We crossed $Apc^{\Delta 716}$ (A), $Kras^{+/LSL\text{-}G12D}$ (K), $Tgfbr2^{flox/flox}$ (T), $Trp53^{+/LSL\text{-}R270H}$ (P), $Fbxw7^{flox/flox}$ (F), and *villin-CreER* mice to generate compound mutant mice carrying driver mutations in different combinations (Fig. 1A and B). These are frequently mutated genes in human colorectal cancer (6, 7). Of note, missense-type mutations of p53 are found in about 50% of human colorectal cancer (6), and we recently showed that mutant $p53^{R270H}$ induces the submucosal invasion of intestinal tumors (22). Accordingly, we used $Trp53^{R270H}$ mice in this study to examine the gain-of-function mechanism of mutant p53. In all mice, intestinal tumors were initiated by somatic loss of wild-type *Apc*, that causes Wnt signaling activation (25). The treatment of compound mice with tamoxifen induced genetic alterations in conditional alleles in an intestinal epithelia-specific manner, and we confirmed the tamoxifen-induced recombination in the intestinal tumor cells (Supplementary Fig. S1).

Although none of compound mice developed spontaneous metastasis (see below), the mean life spans were decreased depending on the increased numbers of driver mutations (Fig. 1C), suggesting that the accumulation of driver mutations affects systemic conditions through secreted factors.

Increased multiplicity of intestinal tumors by $Apc^{\Delta 716}$ $Kras^{G12D}$ combination

We examined the number and size of intestinal polyps in A, AK, AKP, AKT, ATP, AKTP, and AKTPF mice. Intestinal tumors of other genotype mice with the *Fbxw7* mutation were not polypotic and thus uncountable (see below). Notably, the polyp number increased significantly in mice that carried the AK combination, that is, AK, AKP, AKT, AKTP, and AKTPF, in comparison to that in A and ATP mice, indicating that Kras activation increases the multiplicity of tumors (Fig. 1D and E). Interestingly, the ratio of small polyps (<1 mm) dramatically increased in mice carrying AK combination (Fig. 1F), and most small adenomas were located in the upper part of the mucosa without connecting to the crypt bottom (Supplementary Fig. S2). Therefore, these small adenomas in $Kras^{G12D}$ mice may be eliminated by shedding to the lumen, which may explain the increase in the ratio of small polyps. We previously showed that $Apc^{\Delta 716}$ mouse tumor cells cannot survive without generation of COX-2–expressing microenvironment (35, 36). Thus, it is possible that Kras activation contribute to the survival of tumor cells through the generation of such microenvironment.

Submucosal invasion by $Apc^{\Delta 716}$ $Trp53^{R270H}$ and $Apc^{\Delta 716}$ $Tgfbr2^{-/-}$ combinations

Histologic types of all genotype mouse tumors are shown in Supplementary Table S1. Notably, mice carrying AP or AT mutations, that is, AKP, ATP, AKT, ATPF, AKTF, AKTP, and AKTPF mice, developed adenocarcinomas with invasion to submucosa or deeper, while invasive tumors were not found in A, AK, and AKF mice (Fig. 2A and B). These results are consistent with the previous findings that TGFβ signaling suppression or mutant $p53^{R270H}$ expression induces submucosal invasion intestinal tumors (20–22).

Notably, the ratio of stromal volume was significantly increased in the invaded submucosal area with the increased number of αSMA-expressing myofibroblasts in comparison with those in mucosal area regardless of mutation types (Fig. 2A and C). Increased collagen fiber deposition detected by Masson's trichrome staining was consistently found in the submucosal invasion area (Supplementary Fig. S3A). These results indicate that desmoplastic reaction is induced in the submucosa, but not in the mucosa. It has been shown that such fibrotic reactive stroma plays a role in malignant progression through the secretion of various factors including TGFβ and Wnt ligands (37). Tumor cells may therefore acquire malignant characteristics in the submucosa by exposure to desmoplastic microenvironment.

Interestingly, the proliferation rates of tumor cells were significantly lower in the submucosal area than in mucosal area, possibly due to the effect of desmoplastic stroma (Fig. 2D; Supplementary Fig. S3B). We noted no significant difference in the proliferation rates in the mucosa of all genotypes compared with that in simple $Apc^{\Delta 716}$ mouse adenomas, indicating that any of the driver mutations does not accelerate the proliferation in primary tumors.

EMT-like morphology in submucosa and mucosa by distinct combinations

EMT is a hallmark of cancer malignancy (38). We found tumor cell clusters that had lost their glandular architecture and solitary tumor cells in the submucosa, which showed the nuclear

Published OnlineFirst December 27, 2017; DOI: 10.1158/0008-5472.CAN-17-3303

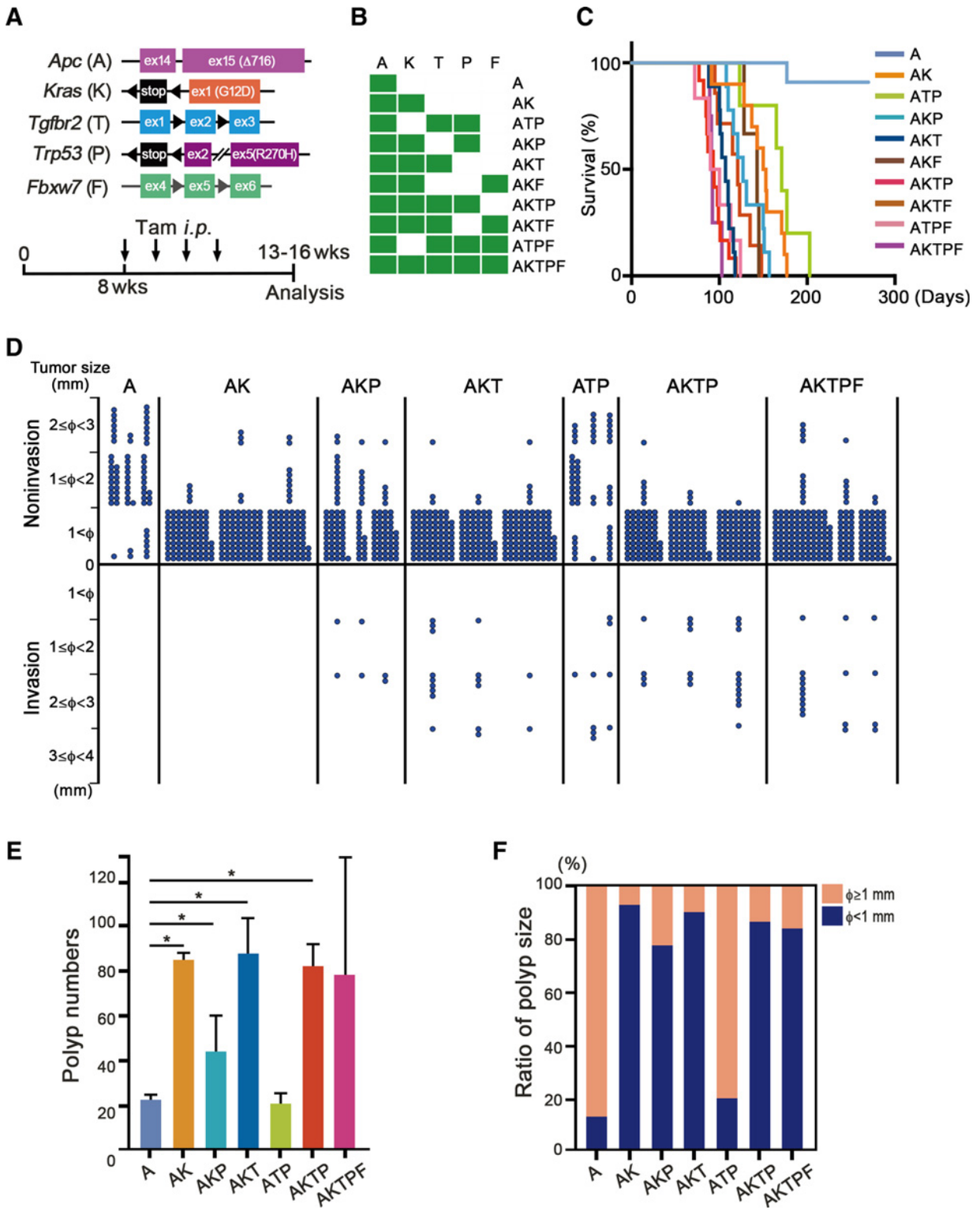

Figure 1.

The generation of mouse models and intestinal polyp phenotypes. **A,** Schematic drawing of mutant alleles of each driver gene (top). Schedule for tamoxifen (Tam) treatment (bottom). **B,** Combinations of driver gene mutations in the respective genotype mice. **C,** The survival curves of each compound mutant strain are shown. **D,** Size classification of noninvasive and invasive intestinal polyps of the indicated compound mutant mice ($n = 3$). Each dot shows an individual polyp. **E,** The number of the intestinal polyps in indicated compound mutant mice (mean ± SD). *, $P < 0.05$. **F,** Ratio of intestinal polyps $\varphi \geq 1$ mm (orange) and $\varphi < 1$ mm (blue) in diameter in the indicated genotype mice.

Published OnlineFirst December 27, 2017; DOI: 10.1158/0008-5472.CAN-17-3303

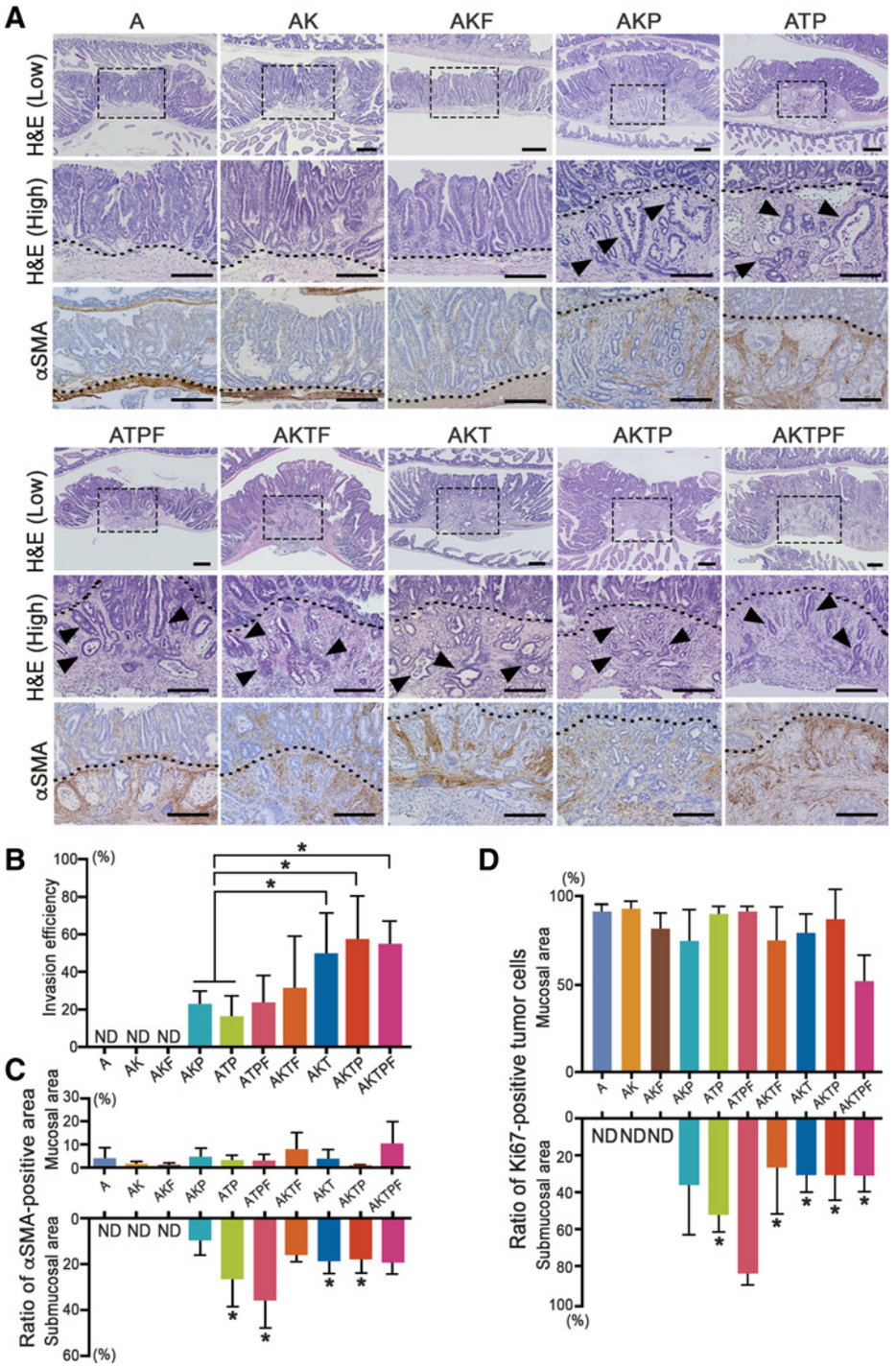

Figure 2.
Submucosal invasion of the primary intestinal tumors in mice carrying AP or AT mutations. **A,** Representative histology sections of the intestinal polyps of the indicated genotype mice (top, H&E low magnification; middle, high magnification of the boxed area in top; bottom, αSMA immunostaining). The dotted lines in middle and bottom indicate the location of the muscularis mucosae. Arrowheads, invading tumor cells in the submucosa. Scale bars, 200 μm. **B,** The efficiency of submucosal invasion in the indicated genotype mice (mean ± SD). ND, not detected. *, $P < 0.05$. **C,** Percentages of αSMA immunostaining–positive area in mucosal (top) and submucosal (bottom) tumors in the indicated genotype mice (mean ± SD). *, $P < 0.05$ versus mucosal area for each genotype. **D,** Percentages of Ki67-positive tumor cells in mucosal (top) and submucosal (bottom) tumors in the indicated genotype mice (mean ± SD). *, $P < 0.05$ versus mucosal area for each genotype.

accumulation of the EMT marker Snail2 (Fig. 3A; Supplementary Fig. S3C). Of note, these invasive tumor cells still expressed E-cadherin, so we classified them as "EMT-like." Importantly, the number of solitary cells in the submucosa was markedly high in AKP, AKT, AKTP, AKTF, and AKTPF mouse tumors that carried AKP or AKT combination but rarely found in ATP and ATPF mice (Fig. 3A and B, right). These results indicate that Kras activation together with mutant $p53^{R270H}$ expression or TGFβ suppression can induce EMT-like morphology when tumor cells are exposed to a desmoplastic microenvironment in submucosa. In contrast, solitary tumor cells were found in the mucosal area of AKF, AKTF, and AKTPF mice that carried AKF combination (Fig. 3A and B, left), suggesting that the combination of *Kras* and *Fbxw7* mutations induces EMT-like morphology without the support of a desmoplastic microenvironment, although AKF combination is not sufficient for invasion.

Published OnlineFirst December 27, 2017; DOI: 10.1158/0008-5472.CAN-17-3303

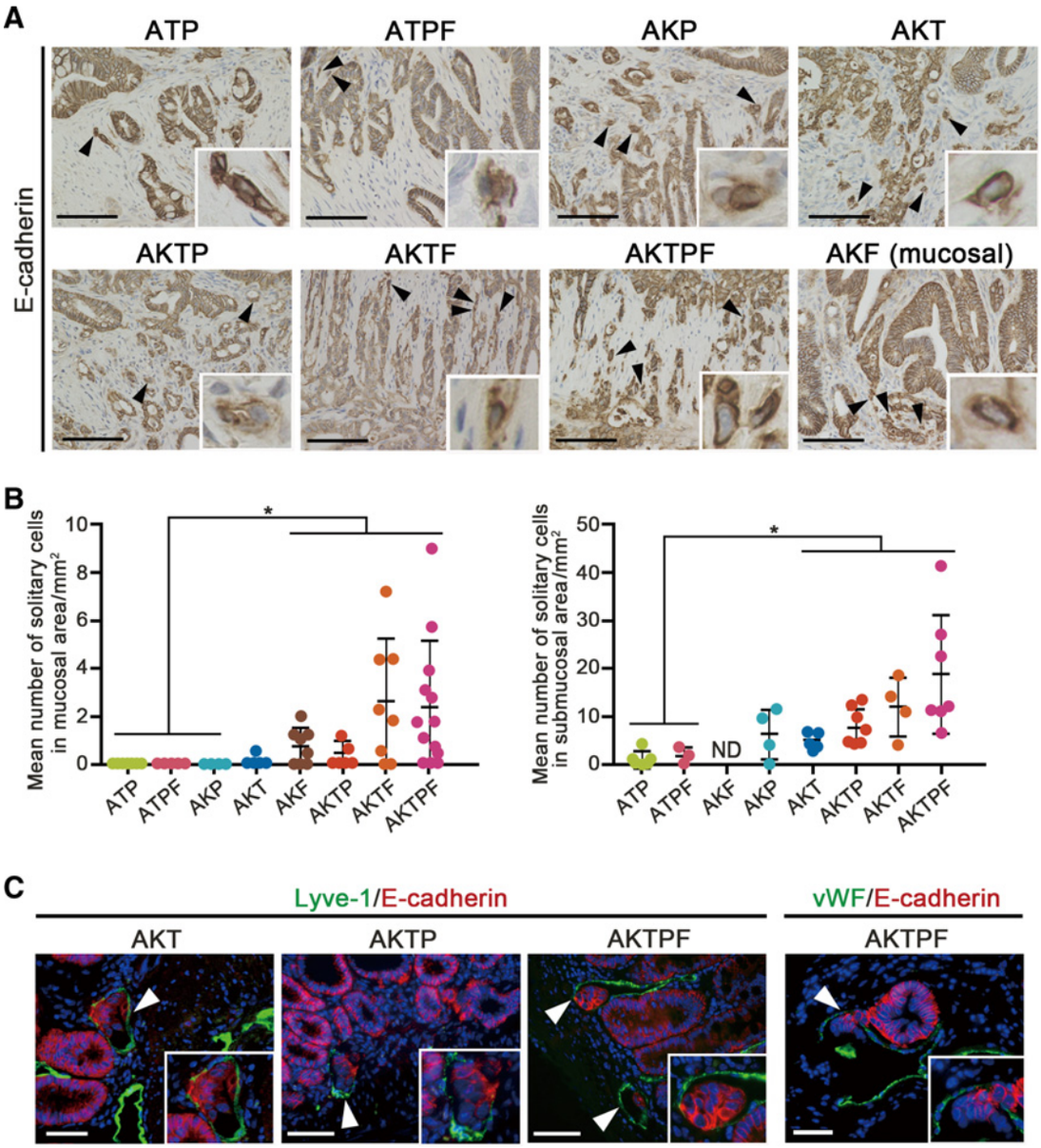

Figure 3.

EMT-like morphology and intravasation of the primary tumors in mice carrying AKP or AKT mutations. **A,** Representative IHC sections for E-cadherin in the submucosal invasion area of AKP, AKT, ATP, AKTP, AKTF, ATPF, and AKTPF mouse tumors and the mucosal area of AKF mouse tumor. The insets indicate enlarged images of solitary or clustered tumor cells. Arrowheads, solitary or clustered tumor cells. Scale bars, 100 μm. **B,** The mean number of solitary tumor cells per mm^2 area in mucosal (left) and submucosal (right) tumors of the indicated genotype mice (mean ± SD). Each dot indicates individual mice. *, $P < 0.05$. **C,** Representative photographs of fluorescence IHC for Lyve-1 or vWF (green), E-cadherin (red), and nuclear counterstaining with DAPI (blue) in the submucosal region of intestinal tumors of the indicated genotype mice. Arrowheads, E-cadherin–positive tumor cells in the Lyve-1–positive lymph vessels or vWF-positive capillary vessel. The insets indicate the enlarged images of tumor cells with intravasation. Scale bars, 200 μm.

Importantly, intravasation into the Lyve-1–expressing lymph vessels was found in AKT, AKTP, and AKTPF mouse tumors but rarely found in other genotype mice (Fig. 3C). Furthermore, intravasation to the blood vessels was also found in the AKTPF mice. The AKT combination may therefore induce intravasation with higher efficiency than the AKP or AKF combination.

Distinct histologic type and accelerated tumorigenesis by $Apc^{\Delta 716}$ $Kras^{G12D}$ $Fbxw7^{-/-}$ combinations

It has been shown that FBXW7 plays a role in the differentiation of intestinal epithelia (16, 17), suggesting that *Fbxw7* mutation may alter the tumor morphology. Interestingly, the histologic type of AKF, AKTF, and AKTPF genotype mouse

Published OnlineFirst December 27, 2017; DOI: 10.1158/0008-5472.CAN-17-3303

tumors that included the AKF combination mutations was villous-type, while other genotype mouse tumors were glandular-type (Supplementary Fig. S4A). Because it was technically difficult to assess the tumor multiplicity of AKF common mice, the tumor distribution was measured by the length ratio on histology sections (Supplementary Fig. S4B). Notably, the tumor distribution was significantly increased in the AKF and AKTF mice compared with other genotype mice that did not carry the AKF combination (Supplementary Fig. S4B and S4C). These results indicate that the combination of Kras activation and *Fbxw7* disruption accelerates tumor growth in addition to inducing EMT-like morphology, and these properties are independent of the invasion ability.

Efficient liver metastasis by the $Apc^{\Delta 716}$ $Kras^{G12D}$ $Tgfbr2^{-/-}$ combination

We detected no spontaneous metastasis in any genotype mice examined, indicating that the accumulation of these driver mutations is not sufficient for metastasis. We therefore established organoids from the tumors of A, AK, AP, AT, ATP, ATPF, AKP, AKT, AKTF, AKTP, and AKTPF mice and transplanted them to the spleens of immunodeficient NSG mice as well as immunocompetent C57BL/6 mice to examine their ability of metastasis to the liver (Fig. 4A). At 4 weeks after spleen injection to NSG mice, tumor organoids with $\geq$3 mutations except for ATP (i.e., AKP, AKT, ATPF, AKTF, AKTP, and AKTPF) developed metastatic tumors with 100% incidence. Among them, the multiplicity of metastasis was significantly higher in the AKT common organoids, that is, AKT, AKTF, AKTP, and AKTPF, than in those of AKP or ATPF (Fig. 4B). The organoids carrying AKT combination efficiently formed metastatic tumors also in C57BL/6 mice, while the incidences of metastasis of AKP and ATPF in C57BL/6 mice were 10% and 0%, respectively (Fig. 4A, C, and D). These results indicate that Wnt activation, Kras activation, and TGFβ suppression by AKT mutations are the core combination for efficient liver metastasis. Notably, additional mutations in *Trp53* and *Fbxw7* to AKT, that is, AKTP and AKTPF, induced the development of lung metastasis after the spleen injection of organoids, which was not found in other genotypes (Fig. 4A). Furthermore, AKTPF organoids showed the highest mean multiplicity of liver metastasis among the AKT common organoids.

Desmoplasia and T-cell infiltration in metastasized tumors

Histologically, metastasized tumors were diagnosed as moderately to poorly differentiated adenocarcinomas with desmoplastic reaction in the stroma consisting of αSMA-positive myofibroblasts (Fig. 4E and F). The desmoplastic reaction was induced in all invaded tumors, suggesting that the AKP or AKT combination is sufficient to induce fibrotic responses in metastatic lesions. In contrast to the primary tumors, the mean proliferation rate of tumor cells increased gradually from AKP to AKT, AKTF, AKTP, and AKTPF (Fig. 4G; Supplementary Fig. S5). Of note, macrophages, $CD4^+$ and $CD8^+$ T cells, and B cells were infiltrated into the metastasized tumors at the similar levels, regardless of the tumor genotypes, whereas T-cell infiltration was rarely found in the primary tumors of the same genotype mice (Fig. 4H and I; Supplementary Fig. S5). Accordingly, the interaction with microenvironment in the metastasized tumors contributes to the induction of the host immune response to tumor cells, although the underlying mechanism remains to be investigated.

Identification of common genes for metastasis induced by the $Apc^{\Delta 716}$ $Kras^{G12D}$ $Tgfbr2^{-/-}$ combination

To examine whether genotype-related malignant phenotypes are associated with distinct expression profiles, we next performed RNA-seq of the tumor organoids for the ATP, AKP, AKT, AKTP, and AKTPF genotypes that showed submucosal invasion in the primary tumors. Notably, a principal component analysis (PCA) indicated that expression profiles of tumors carrying the $Kras^{G12D}$ mutation (AK common, i.e., AKP, AKT, AKTP, and AKTPF) were divergent from that of ATP (Fig. 5A, left), which reflected the fact that Kras activation is required for metastasis. Furthermore, the expression profiles of AKT common (AKT, AKTP, and AKTPF) organoids were distinct from that of AKP (Fig. 5A, center), which reflected the high metastatic ability of AKT common organoids compared with AKP. We also found the evolutional expression changes from AKT to AKTPF via AKTP (Fig. 5A, right). These results suggest that expression changes induced by AKT mutations cause efficient metastasis, and additional mutations in *Trp53* and *Fbxw7* accelerate malignancy, which is consistent with the results of phenotype analyses (Fig. 5B).

We next extracted 363 differentially expressed genes (DEG) in AKT common genotype tumors by selection of overlapping genes in AKT, AKTP, and AKTPF versus A, respectively (Fig. 5C; Supplementary Table S2). GO term analysis using AKT common DEGs indicated significantly enriched pathways relating to angiogenesis, signal transduction, hypoxia, and epithelial morphogenesis, suggesting the role of these pathways in AKT combination-induced metastasis (Fig. 5D). Hierarchical clustering analysis indicated that expression pattern of ATP was divergent from that of AKT common genotypes (Fig. 5E). Although expression of AKP was distinct from AKT common, we found 175 overlapping DEGs in AKT common and AKP but not with ATP (Fig. 5E–G). These results are consistent with those found by PCA (Fig. 5B). Notably, the expression profile of AK tumors was similar to that of AKT common. We found that organoids from AK tumors but not simple $Apc^{\Delta 716}$ tumors formed submucosal tumors with desmoplastic reactions when they were injected directly into colonic submucosa (Supplementary Fig. S6). Taken together, these results suggest that the AK combination significantly contributes to the AKT-induced malignant phenotype.

We thus classified 363 AKT common DEGs to four clusters of AKT (CL1, CL2, CL3, and CL5 in Fig. 5F; Supplementary Table S2), and performed hierarchical clustering analysis. As expected, 73 genes classified to CL5 showed expression patterns specific to the AKT common genotypes, which were not overlapped with AKP and ATP (Fig. 6A and B). Among 73 AKT-common genes, we selected 60 genes, 21 upregulated and 39 downregulated, which were annotated in the TCGA colorectal cancer database, and extracted expression data of these 60 genes. Importantly, the mean expressions of upregulated AKT-common genes were significantly higher in human colorectal cancer with metastasis (M1) than those without metastasis (M0), suggesting that AKT-common signature is important also for human colorectal cancer metastasis (Fig. 6C). Moreover, we found that expression levels of *R3HDML* and *SYT7* were significantly upregulated in M1 than M0 colorectal cancer tissues, while those of *PSME1* and *TMEM150C* were downregulated, which were consistent with those found in the AKT-common profile (Fig. 6B and C). Of note that SYT7, a calcium sensor for synapse exocytosis, plays a role in cell migration (39, 40). Accordingly, it is possible that upregulated genes in

Published OnlineFirst December 27, 2017; DOI: 10.1158/0008-5472.CAN-17-3303

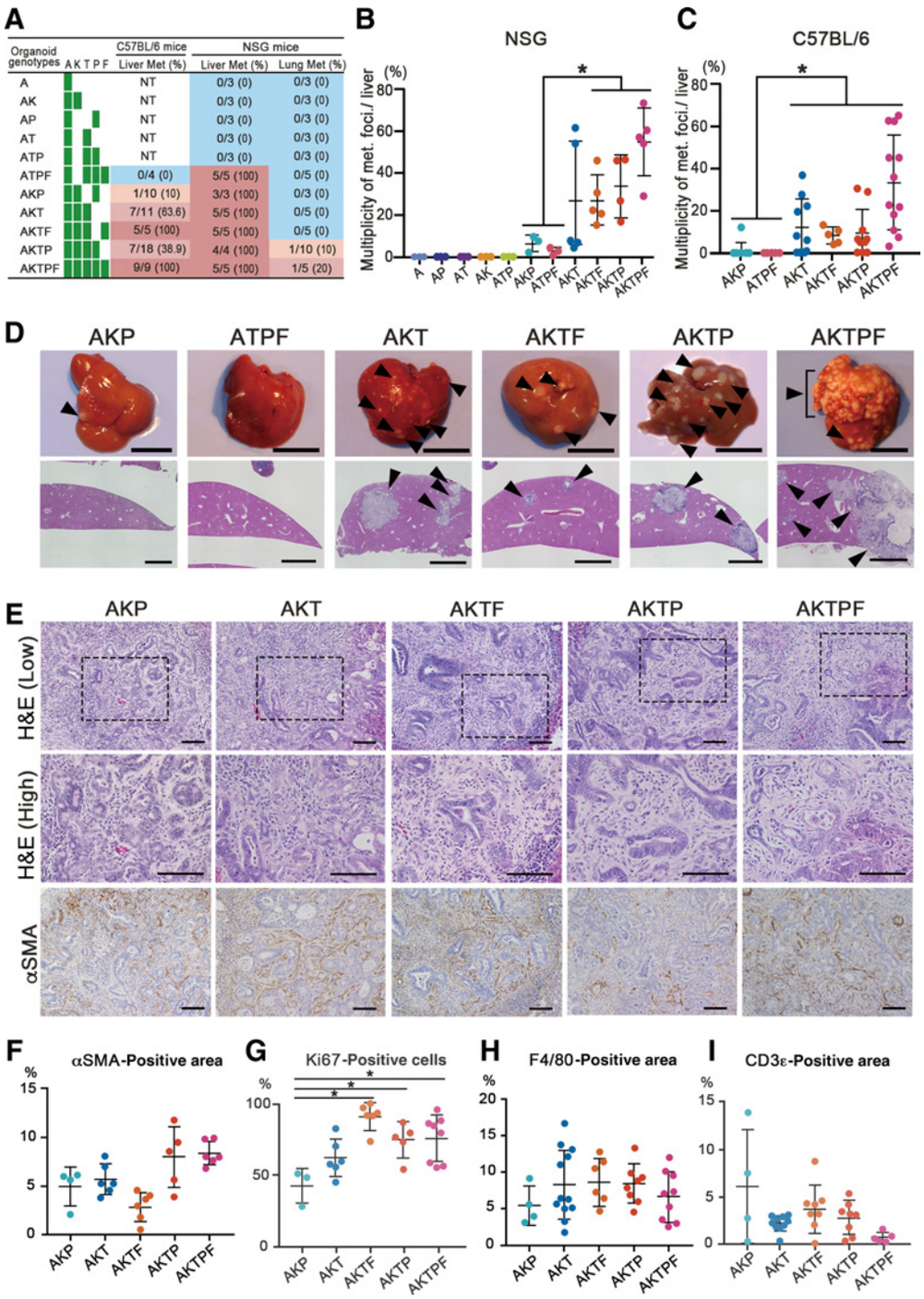

Figure 4.

Liver metastasis of tumor organoids derived from mice carrying AKP and AKT mutations. **A,** Incidence of liver and lung metastasis at 4 weeks after transplantation of the indicated genotype organoids to spleen of C57BL/6 and NSG mice. NT, not tested because of no metastasis in NSG mice. **B** and **C,** Multiplicity of liver metastasis calculated by percentages of metastasized tumor foci in the liver on the H&E sections in NSG mice (**B**) and C57BL/6 mice (mean ± SD; **C**). Each dot indicates individual mice. *, $P < 0.05$. **D,** Representative macroscopic photographs (top) and histology sections (H&E, bottom) of livers of C57BL/6 mice transplanted with the indicated genotype organoids. Arrowheads, metastatic foci. Scale bars, 1 cm (top) and 1 mm (bottom). **E,** Representative photographs of liver metastasis of the indicated genotype organoids in C57BL/6 mice (top, H&E low magnification; middle, enlarged high magnification images of the boxed area in top; bottom, αSMA immunostaining). Scale bars, 200 μm. **F,** Ratio of αSMA immunostaining–positive area in liver metastasis tumors (mean ± SD). **G,** Ratio of Ki67-positive tumor cells in liver metastasis tumors (mean ± SD). **H** and **I,** Ratio of immunostaining-positive area for F4/80 (**H**) and CD3ε (**I**) in liver metastasis tumors (mean ± SD). Each dot indicates individual mice. *, $P < 0.05$.

Published OnlineFirst December 27, 2017; DOI: 10.1158/0008-5472.CAN-17-3303

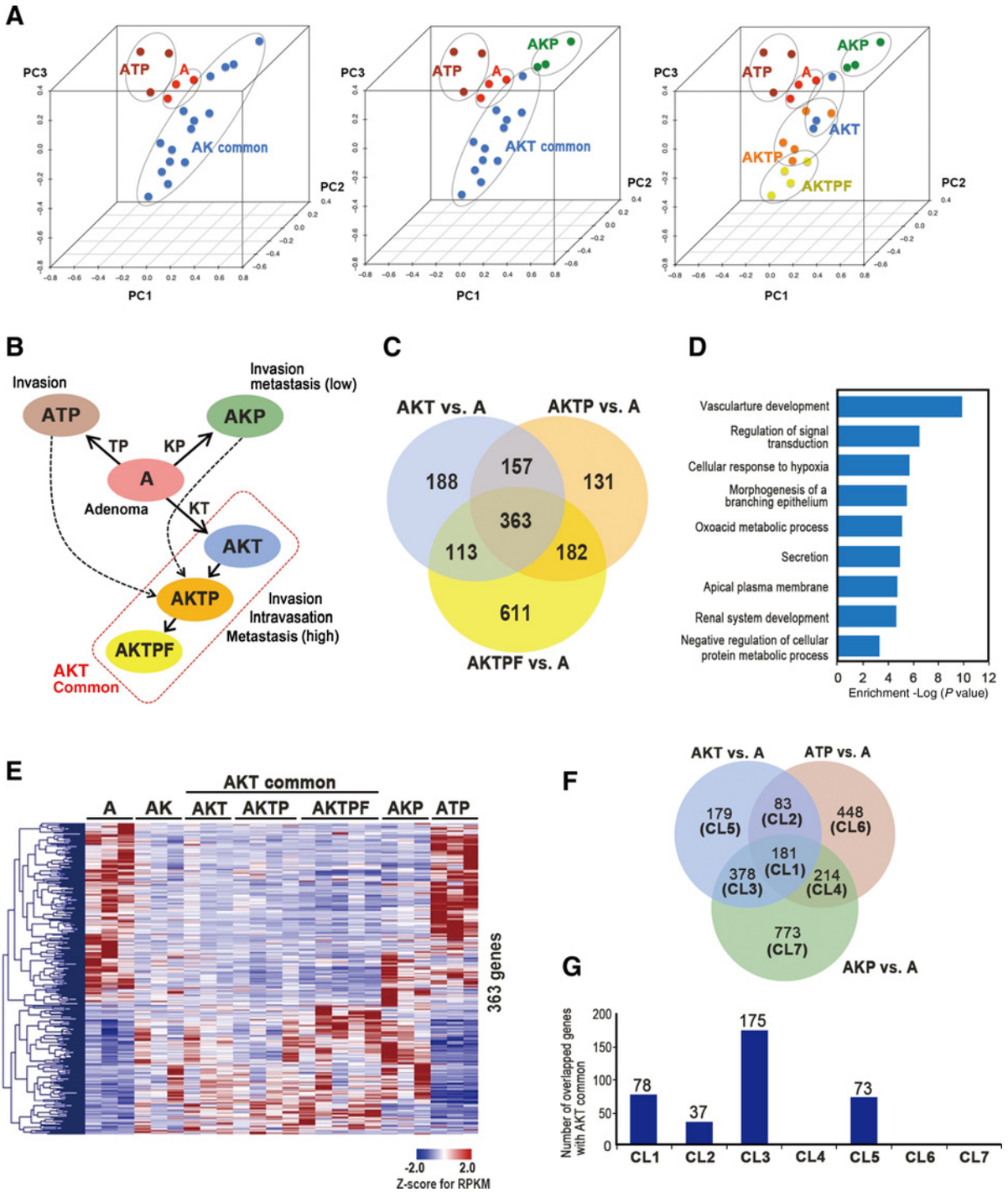

Figure 5.

Gene expression profiles associated with driver mutation-induced malignant progression phenotypes. **A,** A PCA for sequence results of A, ATP, AKP, AKT, AKTP, and AKTPF organoids. AKP, AKT, AKTP, and AKTPF are included in the AK common group (left; blue), and AKT, AKTP, and AKTPF are included in the AKT common group (center; blue). **B,** Schematic model of the evolutionary changes in the gene expression pattern in association with malignant progression phenotypes based on the results of the PCA in **A**. **C,** Venn diagram for overlapping DEGs in AKT, AKTP, and AKTPF versus A. The number of extracted genes and cluster names are indicated. **D,** Functional annotations by GO term analysis using 363 AKT common DEGs are shown (−log of *P* values). **E,** Hierarchical clustering analysis of the AKT common DEGs is shown as fold changes of RPKM compared with the mean. **F,** Venn diagram for overlapping DEGs in AKT, ATP, and AKP versus A. The number of extracted genes and cluster names (CL1–7) are indicated. **G,** The number of AKT common DEGs overlapped in each cluster of AKT DEGs in **F**.

Published OnlineFirst December 27, 2017; DOI: 10.1158/0008-5472.CAN-17-3303

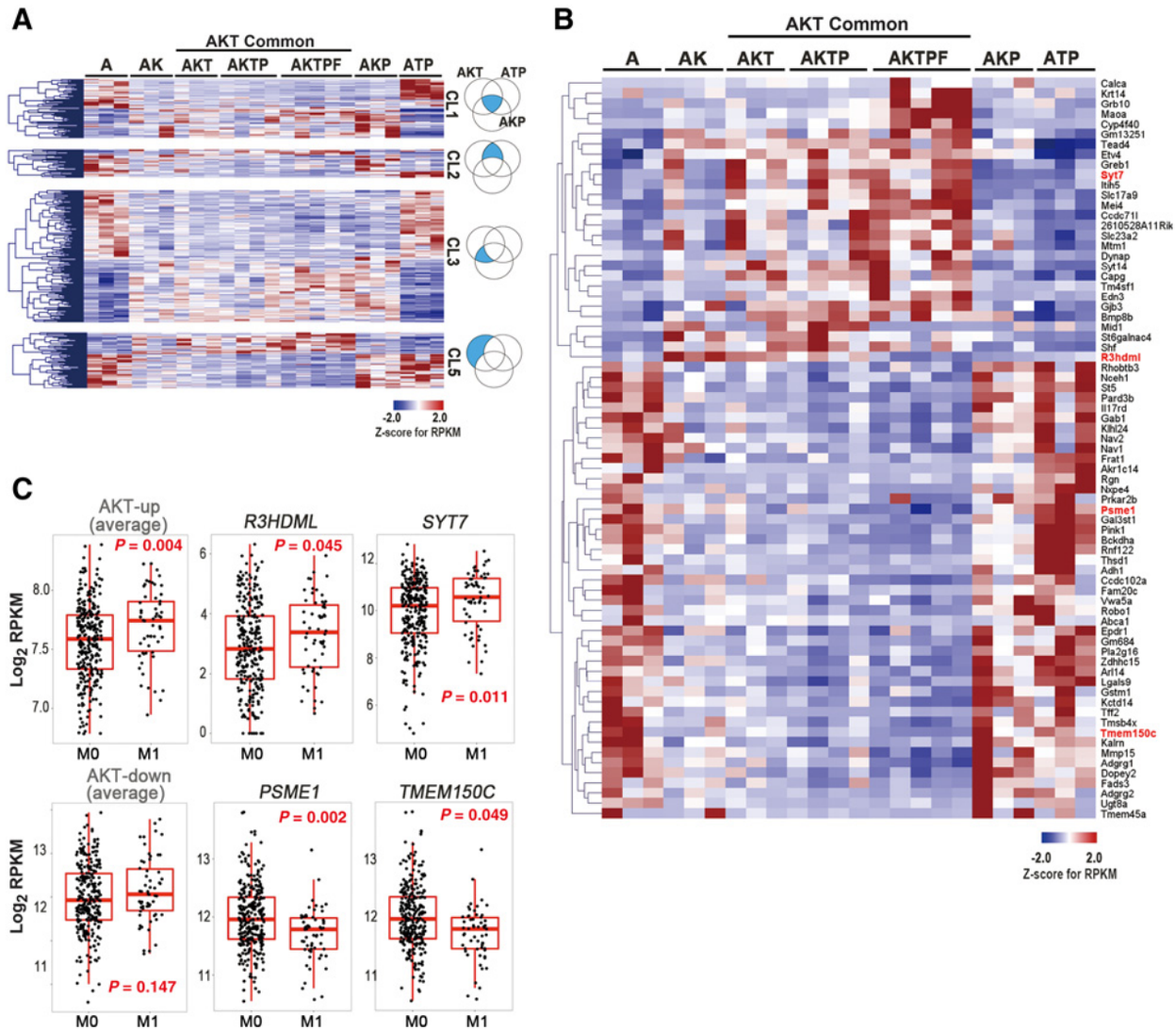

Figure 6.

Extracted DEGs specific to AKT-common genotype tumors. **A,** Hierarchical clustering heatmaps of the AKT-common DEGs that are classified to the respective clusters of AKT (CL1, CL2, CL3, and CL5) are shown as fold changes of RPKM compared with the mean. **B,** The clustering heatmap of the AKT-common DEGs classified to CL5 cluster in **A** is shown with gene symbol. Gene symbols indicated by red are upregulated or downregulated also in human colorectal cancer with metastasis. **C,** Expression analysis of the mean AKT-common upregulated genes (AKT-up) and that of AKT-common downregulated genes (AKT-down), and the indicated genes in human colorectal cancer tissues with metastasis (M1) or without metastasis (M0). *P* values are indicated in red.

AKT-common profile will be effective therapeutic targets for colorectal cancer metastasis.

Discussion

To understand how the specific combinations of driver mutations promote each step for colorectal cancer malignant progression, we performed comprehensive phenotype characterization of the primary intestinal tumors and liver metastasis in mouse models that carried various driver mutations in combination (Fig. 7). Among the driver genes examined in this study, the activation mutation of *Kras* is essential for EMT-like morphology and metastasis. This is consistent with the previous reports that liver and lung metastasis of human colorectal cancer are more likely to develop in patients whose tumors have *KRAS* mutations (41, 42). In addition, a recent genetic study indicated that the continuous expression of activated Kras is required for the maintenance of invasive and metastatic disease (23). In this study, we found that the $Kras^{G12D}$ mutation induced EMT-like morphology of $Apc^{\Delta 716}$ mouse tumors when combined with mutations in either of $Fbxw7^{-/-}$, $Tgfbr2^{-/-}$, or $Trp53^{R270H}$. Furthermore, Kras activation promoted intravasation and efficient liver metastasis when combined with $Apc^{\Delta 716}$ and $Tgfbr2^{-/-}$ mutations (AKT common; Fig. 7). In contrast, the combination of $Apc^{\Delta 716}$ and

Published OnlineFirst December 27, 2017; DOI: 10.1158/0008-5472.CAN-17-3303

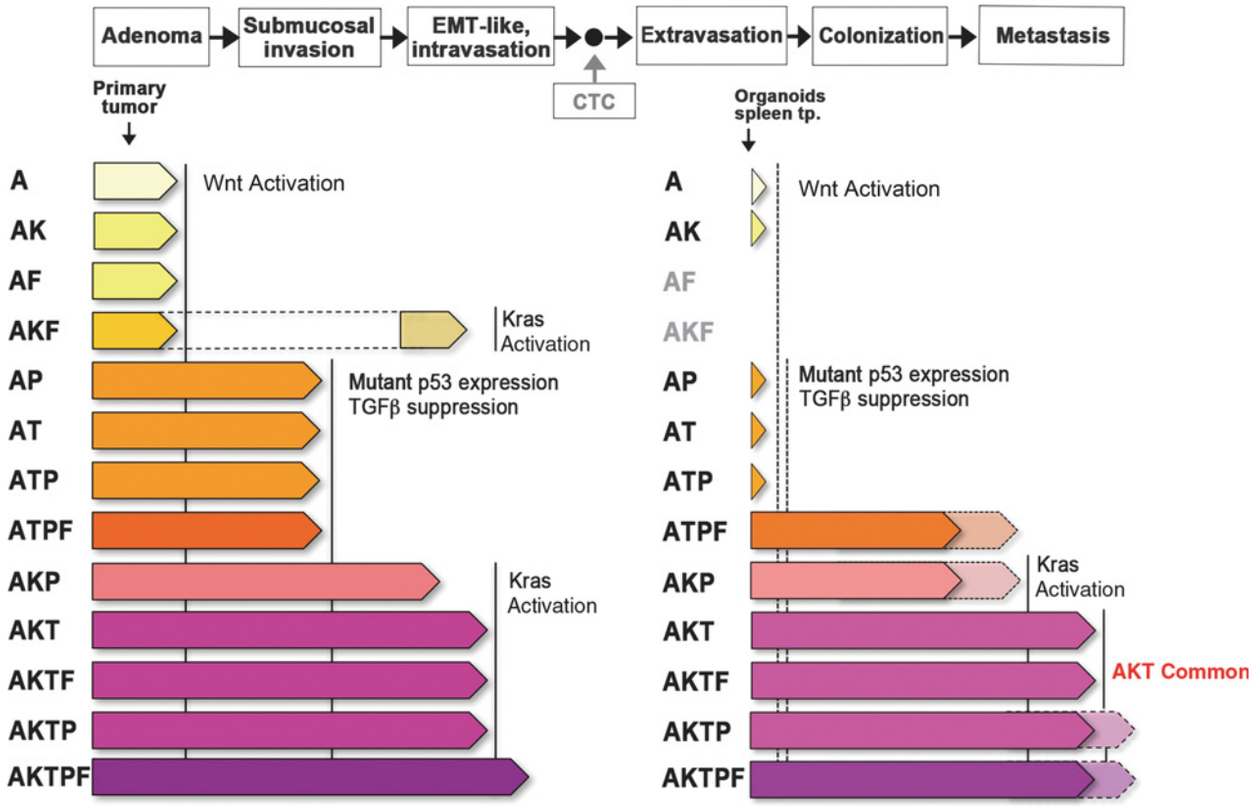

Figure 7.
A schematic drawing of the genotype–phenotype relationship in multistep tumorigenesis. Metastasis phenotypes (right) are based on the results of organoid transplantation to the spleen. AF and AKF were not examined for the metastasis assay (gray). In this study, survival of circulating tumor cells (CTC) was not evaluated for the respective genotypes.

$Kras^{G12D}$ mutations was not sufficient for invasion, indicating that malignant progression by *Kras* mutation requires other driver mutations in combination.

We previously showed that either TGFβ signaling suppression or mutant $p53^{R270H}$ expression induces submucosal invasion of $Apc^{\Delta 716}$ mouse tumors (20–22). Consistently, compound mice that carried AT or AP mutations in their genotypes consistently developed invasive adenocarcinoma. Unexpectedly, however, simultaneous mutations of $Tgfbr2^{-/-}$ and $Trp53^{R270H}$ did not induce further intravasation or metastasis, and the expression profile of ATP organoids was divergent from that of metastatic AKP and AKT organoids. These results confirm the requirement of a *Kras* mutation in addition to either TGFβ suppression (AKT) or p53 mutation (AKP) for metastasis of colorectal cancer (Fig. 7).

On comparing phenotypes between AKP and AKT tumors, AKT showed markedly more advanced malignancy, such as lymph vessel invasion and significantly higher incidence and multiplicity of metastasis in the liver. Interestingly, the expression profiles of AKTP and AKTPF more closely resemble that of AKT than AKP; therefore, we would like to propose that Wnt activation, Kras activation, and TGFβ suppression (i.e., AKT) are core-combination pathways for efficient metastasis, and the selected AKT common DEGs play a role in this process (Fig. 6B). Importantly, the mean expression level of AKT-common upregulated genes was significantly increased in human colorectal cancer with metastasis (M1), suggesting that AKT-common signature is important also for metastasis of human colorectal cancer. Moreover, we found that Syt7 is upregulated both in AKT-common genes and human colorectal cancer with metastasis. Synaptotagmin (Syt) is a well-established calcium sensor for calcium-induced exocytosis of synaptic vesicles (39). Notably, it has been shown that Syt7-mediated vesicle fusion regulates the chemotaxis of leukocytes (40). Accordingly, it is possible that Syt7 plays a tumor-promoting role by accelerating the migration of colorectal cancer cells. Accordingly, activated pathways by AKT-common mutations may play a role in malignant progression of human colorectal cancer.

In contrast, it has been shown that the TGFβ pathway is activated in the invasive tumor cells of *Apc* $Trp53^{Null}$ $Kras^{G12D}$ mice (23) and that TGFβ signaling in the stroma facilitates tumorigenesis through the promotion of fibrosis and immune evasion (43). Accordingly, it is possible that TGFβ signaling in the stroma plays a role in the malignant progression of AKT tumor cells that have lost their TGFβ signaling.

In this study, we also found that a desmoplastic reaction is induced in submucosal tumors and liver metastasis, while such fibrotic reactions were rarely found in noninvading mucosal tumors of the same mice. Notably, the histologic features of tumors were distinctively more malignant in the invasive and metastatic lesions, suggesting that desmoplastic stroma

contributes to the induction of malignant phenotypes. It has been reported that fibrosis with the deposition of type I collagen promotes metastasis by inducing the proliferation of dormant cells via integrin signaling (37, 44, 45), and collagen crosslinking in the stroma results in the promotion of invasion and metastasis (46). Therefore, it is possible that EMT-like morphology and metastasis of AKT tumors are induced by cooperation of driver mutations and fibrotic microenvironment.

The disruption of *Fbxw7* increased the number of intestinal tumors in Apc^{Min} mice (16, 17); however, its role in malignant progression remains unclear. In this study, we showed that the combination of the $Fbxw7^{-/-}$ and $Kras^{G12D}$ mutations (AKF) induced EMT-like morphology in mucosal tumors without the support of fibrotic microenvironment (Fig. 7). It has been shown that Fbxw7 plays a role in stem cell regulation, and its deletion accelerates the self-renewal activity of stem cells (47). Furthermore, there is a direct link between EMT and the gain of epithelial stem cell properties (48). It is therefore possible that *Fbxw7* disruption leads to EMT-like morphology through the acquisition of stem cell properties, which may contribute to the increased multiplicity of metastasis of AKTPF tumors compared with AKTP.

In this study, we did not find spontaneous metastasis to distant organs in any genotype mice, even if tumor cells can invade into vessels and metastasize to liver from spleen (Fig. 7). It is therefore possible that additional genetic or epigenetic alteration(s) are required to overcome physical stresses in the blood stream and escape from immune attack, which are required to be survived as circulating tumor cells (Fig. 7; ref. 37).

Microsatellite instability (MSI)-high colorectal cancer is associated with an increased level of immune cell infiltration (49), therefore, MSI-high colorectal cancer responds to immune checkpoint blockade (50). However, the association with tumor-infiltrating lymphocytes was also evident in microsatellite-stable colorectal cancer tumors (7), indicating that non-MSI colorectal cancer also can induce an immune reaction. In this study, we found that both $CD4^+$ and $CD8^+$ T cells infiltrated into metastasized tumors of C57BL/6 mice at the similar level among all genotypes, although T-cell infiltration was rarely detected even in the invasive area of the primary tumors. These results suggest a mechanism of the microenvironment in the metastasized tumors to induce immune responses against non-MSI colorectal cancer cells, although further studies will be needed. This mechanism is particularly important for understanding tumor immunity, which will help develop therapeutic strategies for preventing colorectal cancer metastasis in the future.

In conclusion, we constructed mouse models with multiple combinations of driver mutations and performed the comprehensive characterization of the primary and metastatic tumors. Suppression of the TGFβ pathway or expression of mutant p53 induces submucosal invasion, and additional *Kras* mutation activation is required for further malignant progression including EMT-like morphology, intravasation, and metastasis. In contrast, the combination of Fbxw7 inhibition and Kras activation induces EMT-like morphology, possibly through increased stemness. Finally, Wnt activation, Kras activation, and TGFβ suppression represent important combination for efficient metastasis, which is corroborated by the RNA-seq analysis. Accordingly, pathways activated by the AKT-common DEGs may be preventive or therapeutic targets against colorectal cancer metastasis.

Disclosure of Potential Conflicts of Interest

No potential conflicts of interest were disclosed.

Authors' Contributions

Conception and design: M. Oshima

Acquisition of data (provided animals, acquired and managed patients, provided facilities, etc.): E. Sakai, H. Oshima, S. Fujii, A. Ochiai, Y. Suzuki

Analysis and interpretation of data (e.g., statistical analysis, biostatistics, computational analysis): M. Nakayama, Y. Kouyama, A. Niida, K. Mimori, C.P. Hong, C.-Y. Ock, S.-J. Kim

Writing, review, and/or revision of the manuscript: S. Fujii, C.-Y. Ock, M. Oshima

Administrative, technical, or material support (i.e., reporting or organizing data, constructing databases): K.I. Nakayama

Study supervision: K.I. Nakayama, M. Oshima

Acknowledgments

This work was supported by grants from AMED-CREST, AMED, Japan Agency for Medical Research and Development, Japan and Grants-in-Aid for Scientific Research (A) (15H02362), (C) (26430110), Innovative Areas (17H05616) and (16H06279) from the Ministry of Education, Culture, Sports, Science and Technology of Japan. We thank Yoshie Jomen, Ayako Tsuda, and Manami Watanabe for their technical assistance.

The costs of publication of this article were defrayed in part by the payment of page charges. This article must therefore be hereby marked *advertisement* in accordance with 18 U.S.C. Section 1734 solely to indicate this fact.

Received October 24, 2017; revised December 6, 2017; accepted December 21, 2017; published OnlineFirst December 27, 2017.

References

1. Ferlay J, Steliarova-Foucher E, Lortet-Tieulent J, Rosso S, Coebergh JWW, Comber H, et al. Cancer incidence and mortality patterns in Europe: estimates for 40 countries in 2012. Eur J Cancer 2013;49:1374–403.
2. Siegel R, Desantis C, Jemal A. Colorectal cancer statistics, 2014. CA Cancer J Clin 2014;64:104–17.
3. Howlader N, Noone AM, Krapcho M, Miller D, Bishop K, Kosary CL, et al. SEER cancer statistics review, 1975–2014. Bethesda, MD: National Cancer Institute; 2017.
4. Markowitz SD, Bertagnolli MM. Molecular origins of cancer: Molecular basis of colorectal cancer. N Engl J Med 2009;361:2449–60.
5. Garraway LA, Lander ES. Lessons from the cancer genome. Cell 2013;153:17–37.
6. The Cancer Genome Atlas Network. Comprehensive molecular characterization of human colon and rectal cancer. Nature 2012;487:330–7.
7. Giannakis M, Mu XJ, Shukla SA, Qian ZR, Cohen O, Nishihara R, et al. Genomic correlates of immune-cell infiltrates in colorectal carcinoma. Cell Rep 2016;15:857–65.
8. Li X, Nadauld L, Ootani A, Corney DC, Pai RK, Gevaert O, et al. Oncogenic transformation of diverse gastrointestinal tissues in primary organoid culture. Nat Med 2014;20:769–77.
9. Matano M, Date S, Shimokawa M, Takano A, Fujii M, Ohta Y, et al. Modeling colorectal cancer using CRISPR-Cas9-mediated engineering of human intestinal organoids. Nat Med 2015;21:256–62.
10. Drost J, van Jaarsveld RH, Ponsioen B, Zimberlin C, van Boxtel R, Buijs A, et al. Sequential cancer mutations in cultured human intestinal stem cells. Nature 2015;521:43–7.
11. Vogelstein B, Papadopoulos N, Velculescu VE, Zhou S, Diaz LA Jr, Kinzler EW. Cancer genome landscapes. Science 2013;339:1546–58.
12. Clevers H, Nusse R. Wnt/β-catenin signaling and disease. Cell 2012;149:1192–205.

13. McCormick F. KRAS as a therapeutic target. Clin Cancer Res 2015;21: 1797–801.
14. Jung B, Staudacher JJ, Beauchamp D. Transforming growth factor β superfamily signaling in development of colorectal cancer. Gastroenterology 2017;152:36–52.
15. Welcker M, Clurman BE. FBW7 ubiquitin ligase: a tumour suppressor at the crossroads of cell division, growth and differentiation. Nat Rev Cancer 2008;8:83–93.
16. Sancho R, Jandke A, Davis H, Diefenbacher ME, Tomlinson I, Behrens A. F-box and WD repeat domain-containing 7 regulates intestinal cell lineage commitment and is a haploinsufficient tumor suppressor. Gastroenterology 2010;139:929–41.
17. Babaei-Jadidi, Li N, Saadeddin A, Spencer-Dene B, Jandke A, Muhammad B, et al. FBXW7 influences murine intestinal homeostasis and cancer, targeting Notch, Jun, and DEK for degradation. J Exp Med 2011;208: 295–312.
18. Pfister NT, Fomin V, Regunath K, Zhou JY, Zhou W, Silwal-Pandit L, et al. Mutant p53 cooperates with the SWI/SNF chromatin remodeling complex to regulate VEGF2 in breast cancer cells. Genes Dev 2015; 29:1298–315.
19. Zhu J, Sammons MA, Donahue G, Dou Z, Vedadi M, Getlik M, et al. Gain-of-function p53 mutants co-opt chromatin pathways to drive cancer growth. Nature 2015;525:206–11.
20. Kitamura T, Kometani K, Hashida H, Matsunaga A, Miyoshi H, Hosogi H, et al. SMAD4-deficient intestinal tumors recruit CCR1+ myeloid cells that promote invasion. Nat Genet 2007;39:465–75.
21. Oshima H, Nakayama M, Han TS, Naoi K, Ju X, Maeda Y, et al. Suppressing TGFβ signaling in regenerating epithelia in an inflammatory microenvironment is sufficient to cause invasive intestinal cancer. Cancer Res 2015;75:766–76.
22. Nakayama M, Sakai E, Echizen K, Yamada Y, Oshima H, Han TS, et al. Intestinal cancer progression by mutant p53 through the acquisition of invasiveness associated with complex glandular structure formation. Oncogene 2017;36:5885–96.
23. Boutin AT, Liao WT, Wang M, Hwang SS, Karpinets TV, Cheung H, et al. Oncogenic Kras drives invasion and maintains metastasis in colorectal cancer. Genes Dev 2017;31:370–82.
24. Roper J, Tammela T, Cetinbas NM, Akkad A, Roghanian A, Rickelt S, et al. In vivo genome editing and organoid transplantation models of colorectal cancer metastasis. Nat Biotech 2017;35:569–76.
25. Oshima M, Oshima H, Kitagawa K, Kobayashi M, Itakura C, Taketo M. Loss of Apc heterozygosity and abnormal tissue building in nascent intestinal polyps in mice carrying a truncated Apc gene. Proc Natl Acad Sci U S A 1995;92:4482–6.
26. Onoyama I, Tsunematsu R, Matsumoto A, Kimura T, de Alborán IM, Nakayama K, et al. Conditional inactivation of Fbxw7 impairs cell-cycle exit during T cell differentiation and results in lymphomatogenesis. J Exp Med 2007;204:2875–88.
27. el Marjou F, Janssen KP, Chang BH, Li M, Hindie V, Chan L, et al. Tissue-specific and inducible Cre-mediated recombination in the gut epithelium. Genesis 2004;39:186–93.
28. Chytil A, Magnunson MA, Wright CV, Moses HL. Conditional inactivation of the TGF-β type II receptor using Cre:Lox. Genesis 2002;32: 73–5.
29. Olive KP, Tuveson DA, Ruhe ZC, Yin B, Willis NA, Bronson RT, et al. Mutant p53 gain of function in two mouse models of Li-Fraumeni syndrome. Cell 2004;119:847–60.
30. Jackson EL, Willis N, Mercer K, Bronson RT, Crowley D, Montoya R, et al. Analysis of lung tumor initiation and progression using conditional expression of oncogenic K-ras. Genes Dev 2001;15:3243–8.
31. Japanese Society for Cancer of the Colon and Rectum. In: Japanese classification of colorectal carcinoma. Second English Edition. Tokyo, Japan: Kanehara & Co., Ltd; 2009. Available at http://www.jsccr.jp/en/jccc.html
32. Kim D, Pertea G, Trapnell C, Pimentel H, Kelley R, Salzberg SL. TopHat2: accurate alignment of transcriptomes in the presence of insertions, deletions and gene fusions. Genome Biol 2013;14:R36.
33. Trapnell C, Williams BA, Pertea G, Mortazavi A, Kwan G, van Baren MJ, et al. Transcript assembly and quantification by RNA-Seq reveals unannotated transcripts and isoform switching during cell differentiation. Nat Biotech 2010;28:511–5.
34. Huang DW, Sherman BT, Lempicki RA. Systematic and integrative analysis of large gene lists using DAVID bioinformatics resources. Nat Protoc 2009;4:44–57.
35. Oshima M, Dinchuk JE, Kargman SL, Oshima H, Hancock B, Kwong E, et al. Suppression of intestinal polyposis in Apcδ716 knockout mice by inhibition of cyclooxygenase 2 (COX-2). Cell 1996;87:803–9.
36. Oshima M, Murai N, Kargman S, Arguello M, Luk P, Kwong E, et al. Chemoprevention of intestinal polyposis in the Apcδ716 mouse by rofecoxib, a specific cyclooxigenase-2 inhibitor. Cancer Res 2001;61:1733–40.
37. Lambert AW, Pattabiraman DR, Weinberg RA. Emerging biological principles of metastasis. Cell 2017;168:670–91.
38. Polyak K, Weinberg RA. Transitions between epithelial and mesenchymal states: acquisition of malignant and stem cell traits. Nat Rev Cancer 2009;9:265–73.
39. Sudhof TC. Neurotransmitter release: the last millisecond in the life of a synaptic vesicle. Neuron 2013;80:675–90.
40. Colvin RA, Means TK, Diefenbach TJ, Moita LF, Friday RP, Sever S, et al. Synaptotagmin-mediated vesicle fusion regulates cell migration. Nat Immunol 2010;22:495–502.
41. Knijn N, Mekenkamp LJ, Klomp M, Vink-Börger ME, Tol J, Teerenstra S, et al. KRAS mutation analysis: a comparison between primary tumours and matched liver metastasis in 305 colorectal cancer patients. Br J Cancer 2011;104:1020–6.
42. Pereira AA, Rego JF, Morris V, Overman MJ, Eng C, Garrett CR, et al. Association between KRAS mutation and lung metastasis in advanced colorectal cancer. Br J Cancer 2015;112:424–8.
43. Principe DR, DeCant B, Mascarinas E, Wayne EA, Diaz AM, Akagi N, et al. TGFβ signaling in the pancreatic tumor microenvironment promotes fibrosis and immune evasion to facilitate tumorigenesis. Cancer Res 2016;76:2525–39.
44. Barkan D, El Touny LH, Michalowski AM, Smith JA, Chu I, Davis AS, et al. Metastatic growth from dormant cells induced by a Col-I-enriched fibrotic environment. Cancer Res 2010;70:5706–16.
45. Cox TR, Erler JT. Molecular pathways: connecting fibrosis and solid tumor metastasis. Clin Cancer Res 2014;20:3637–43.
46. Levental KR, Yu H, Kass L, Lakins JN, Egeblad M, Erier JT, et al. Matrix crosslinking forces tumor progression by enhancing integrin signaling. Cell 2009;139:891–906.
47. Takeishi S, Nakayama KI. Role of Fbxw7 in the maintenance of normal stem cells and cancer-initiating cells. Br J Cancer 2014;111:1054–9.
48. Mani SA, Guo W, Liao MJ, Eaton EN, Ayyanan A, Zhou AY, et al. The epithelial-mesenchymal transition generates cells with properties of stem cells. Cell 2008;133:704–15.
49. Jass J, Do K, Simms L, Iino H, Wynter C, Pillay S, et al. Morphology of sporadic colorectal cancer with DNA replication errors. Gut 1998;42: 673–9.
50. Le DT, Uram JN, Wang H, Bartlett BR, Kemberling H, Eyring AD, et al. PD-1 blockade in tumors with mismatch-repair deficiency. N Engl J Med 2015;372:2509–20.

Published OnlineFirst December 27, 2017; DOI: 10.1158/0008-5472.CAN-17-3303

Cancer Research
The Journal of Cancer Research (1916–1930) | The American Journal of Cancer (1931–1940)

AACR American Association for Cancer Research

Combined Mutation of *Apc, Kras*, and *Tgfbr2* Effectively Drives Metastasis of Intestinal Cancer

Eri Sakai, Mizuho Nakayama, Hiroko Oshima, et al.

Cancer Res 2018;78:1334-1346. Published OnlineFirst December 27, 2017.